Published in IET Microwaves, Antennas & Propagation
Received on 11th March 2014
Revised on 10th June 2014
Accepted on 3rd July 2014
doi: 10.1049/iet-map.2014.0163

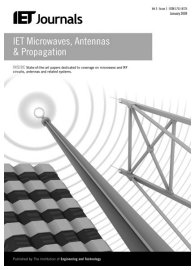

ISSN 1751-8725

Measurement and analysis of the lowest resonant mode of a spherical annular-sector patch antenna

Steven Weiss[1], *Howard Cohl*[2], *Amang Boliong*[3]

[1]*AMSRL-SER-M, The Army Research Laboratory, Adelphi, MD 20783, USA*
[2]*Applied and Computational Mathematics, National Institute of Standards and Technology, Gaithersburg, MD 20899-8910, USA*
[3]*Department of Electrical Engineering, The Morgan State University, Baltimore, MD 21251, USA*
E-mail: steven.j.weiss14.civ@mail.mil

Abstract: The cavity model for patch antennas has been used extensively since 1970s. This model gives excellent first-order estimates for the antenna's internal fields near any resonant frequency. Although frequently used for planar geometries, there is no reason why the model cannot be employed for other geometries. This study discusses some of the complexities in selecting the correct pair of linearly independent associated Legendre functions when attempting to employ the cavity model using a spherical annular-sector patch antenna.

1 Introduction

It is well known and established that the resonant frequencies for patch antennas can be analytically determined through the use of the cavity model [1]. This model estimates the shape of the patch antenna's internal fields by solving a boundary value problem that presumes magnetic walls about the perimeter of the patch and electric walls on the top (the patch antenna) and bottom (the ground plane). The analytical procedures are well known and extricate the resonant modes [1].

Although the cavity model is commonly employed in Cartesian, cylindrical and (less frequently) elliptic cylinder coordinates, there is no inherent limitation for geometries that have ground planes with non-vanishing curvature [2–4]. The motivation for this paper pertains to reconciling the 'measured' (lowest) resonant frequency of a spherical annular-sector antenna with analytical predictions for the lowest resonance. Accordingly, this paper reviews the separation of variables procedure for finding the resonant modes of an annular-sector patch antenna (sometimes called a spherical-rectangular microstrip antenna [5–7]) on a curved (spherical) ground plane paying particular attention to the choice of associated Legendre functions.

Patch antennas over a spherical conducting surface are not as frequently used as a patch antenna over a planar surface; however, there are applications for which this type of antenna is needed. For example, the helmet of a soldier can be considered nearly spherical and the analysis of this paper would then apply. Of course, proper layering with a spherical patch antenna over conducting support would need to be integrated into the helmet. Besides military applications, many emergency service personnel and recreational sporting activities require the use of protective helmets for which this analysis would also be pertinent.

Estimates for resonant modes (and the corresponding resonant frequencies) of the annular sector can be approximated presuming a rectangular patch on a planar surface. However, when placed on a spherical surface, the sides of the patch are then described in terms of arc lengths that do not directly correspond to the lengths of the rectangular sides introducing error in the calculation of the resonant frequencies.

It is through the use of analytical techniques that one gains valuable understanding into the shape of the antenna's internal fields; a perspective that is of value in its own right. The insight from this analytic perspective is not necessarily gained from computer simulations arriving at similar results (e.g. the same resonant frequency); although computer simulations have shown good correspondence with measurement [7–10]. Additionally, analytical techniques provide good first-order estimates of the angular spans in azimuth and elevation for achieving a desired resonant frequency-saving computer simulation time. This paper addresses some of the analytical complexities encountered in determining the lowest resonant mode of the spherical annular-sector patch antenna comparing the results to measured data.

A spherical annular-sector patch antenna shown in Fig. 1 was constructed [10–12], and is studied in this paper. For the parameters shown in Fig. 1, the angular span in azimuth is: $\phi_1 = 0°$ and $\phi_2 = 130.4°$, whereas the span for the elevation angle is: $\theta_1 = 36.2°$ and $\theta_2 = 60.9°$. The inner (the surface of the ground plane) and outer (the patch antenna) radii are: $a = 15.329$ cm and $b = 15.393$ cm.

The antenna depicted in Fig. 1 was fabricated and fed with a probe, Fig. 2. The lowest measured resonant frequency was found to be 442.0 MHz, Fig. 3. The dielectric between the patch and ground plane was polyethylene terephthalate glycol (PETG with $\varepsilon_r = 2.3$).

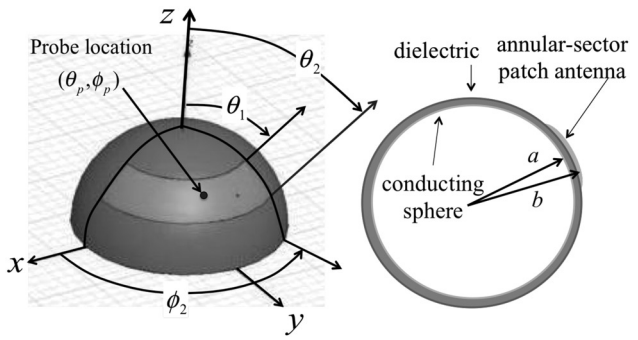

Fig. 1 *Spherical annular-sector patch antenna*

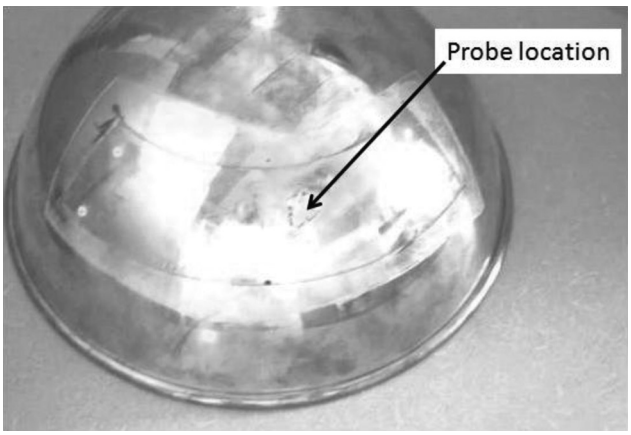

Fig. 2 *Prototype spherical annular-sector antenna with the probe located at $\theta_p = 42°$ and $\phi_p = 70°$*

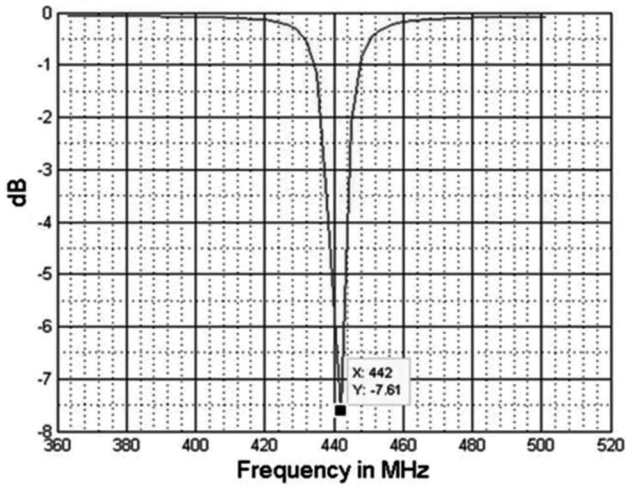

Fig. 3 *Measured reflection coefficient at the probe location for the annular-sector antenna against frequency*

2 Formulation of the problem

As indicated, the cavity model yields solutions for the electric and magnetic fields underneath the patch in spherical coordinates. These fields can be found presuming a transverse magnetic (TM, derivable from the radial component of the magnetic vector potential, $\boldsymbol{A}_r$) and a transverse electric (TE, derivable from the radial component of the electric vector potential, $\boldsymbol{F}_r$) decomposition [13, 14]. This being stated, the lowest resonant frequencies are identified through the TM analysis for which this paper will focus entirely. The TM electric and magnetic fields are found by differentiating the vector potential $\boldsymbol{A}_r$ [13, p. 550, (10–27)–(10–28)]

$$E_\theta = \frac{1}{\mathrm{j}\omega\varepsilon\mu}\frac{1}{r}\frac{\partial^2 A_r}{\partial r\partial\theta}, \quad H_\theta = \frac{1}{\mu}\frac{1}{r\sin\theta}\frac{\partial A_r}{\partial\phi}$$

$$E_\phi = \frac{1}{\mathrm{j}\omega\varepsilon\mu}\frac{1}{r\sin\theta}\frac{\partial^2 A_r}{\partial r\partial\phi}, \quad H_\phi = -\frac{1}{\mu}\frac{1}{r}\frac{\partial A_r}{\partial\theta} \tag{1}$$

$$E_r = \frac{1}{\mathrm{j}\omega\varepsilon\mu}\left[\frac{\partial^2 A_r}{\partial r^2} + k^2 A_r\right], \quad H_r = 0$$

The radial component A_r/r satisfies the scalar Helmholtz equation with the homogenous solution found using separation of variables. Accordingly, the general separable solution of interest can be given by

$$\begin{aligned} A_r = \sum_{\nu\in\nu'}\sum_{\alpha\in\alpha'} A_{\alpha\nu}\big(C_1\cos(\alpha\phi) + C_2\sin(\alpha\phi)\big) \\ \times\big(C_3 P_\nu^\alpha(\cos\theta) + C_4 Q_\nu^\alpha(\cos\theta)\big) \\ \times\big(C_5\hat{j}_\nu(kr) + C_6\hat{y}_\nu(kr)\big) \end{aligned} \tag{2}$$

where ν' and α' are countable infinite sets depending on the geometry of the problem. In (2), $P_\nu^\alpha(\cos\theta)$ and $Q_\nu^\alpha(\cos\theta)$ are commonly used associated Legendre functions (Ferrers functions [15, 14.2(ii)]) of the first and second kind, respectively, of degree ν and order α. The variable α is the separation constant associated with the azimuthal angle ϕ. Note the use of Schelkunoff's spherical Bessel functions $\hat{j}_\nu(kr)$ and $\hat{y}_\nu(kr)$ in (2) [13, p. 551, (10–31)].

The solution of the TM problem reduces to determination of the various constants in (2). This paper provides a study of implications when the selection of the associated Legendre function pair $P_\nu^\alpha(x)$ and $Q_\nu^\alpha(x)$ is used and describes the need for alternate pairs when trying to reconcile the lowest measured resonant frequency with analytical predictions.

3 Analytical calculation of the lowest resonant frequency using the cavity model

In accordance with the magnetic walls of the cavity model, the magnetic fields in the H_θ must vanish at ϕ_1 and ϕ_2 since this magnetic field component is tangent to these walls. H_θ is found by differentiating (2) with respect to ϕ in accordance with (1). Enforcing the boundary condition that H_θ must vanish at $\phi_1 = 0°$ is met by the adjustment of the constants such that $C_1 = 1$ and $C_2 = 0$. Enforcing the boundary condition that H_θ must vanish at $\phi_2 = 130.4°$ is met by setting the separation constant α equal to discrete values (eigenvalues). That is, $\alpha = m\pi/\phi_2 \cong 1.38037\,m$, where $m = 1, 2, \ldots$.

The magnetic field component H_ϕ is tangent to the magnetic walls at θ_1 and θ_2, and must vanish in accordance with the cavity model. Again, we differentiate (2) in accordance with (1) (i.e. with respect to θ) to find H_ϕ. The boundary condition that H_ϕ vanishes at θ_2 can be accomplished with the adjustment of constants, that is

$$C_3 = \left[\frac{\mathrm{d}}{\mathrm{d}\,\theta}Q_\nu^\alpha(\cos\theta)\right]_{\theta=\theta_2} \quad \text{and} \quad C_4 = \left[\frac{\mathrm{d}}{\mathrm{d}\,\theta}P_\nu^\alpha(\cos\theta)\right]_{\theta=\theta_2}$$

doi: 10.1049/iet-map.2014.0163

The requirement that H_ϕ vanishes at θ_1 can only be enforced by the proper selection of the degree ν. To this end, we may plot (using Mathematica) the function

$$f_\alpha^{(\theta_1,\theta_2)}(\nu) = \left[\frac{\mathrm{d}}{\mathrm{d}\,\theta}P_\nu^\alpha(\cos\,\theta)\right]_{\theta=\theta_1} - \left[\frac{\mathrm{d}}{\mathrm{d}\,\theta}Q_\nu^\alpha(\cos\,\theta)\right]_{\theta=\theta_2} - \left[\frac{\mathrm{d}}{\mathrm{d}\,\theta}Q_\nu^\alpha(\cos\,\theta)\right]_{\theta=\theta_1}\left[\frac{\mathrm{d}}{\mathrm{d}\,\theta}P_\nu^\alpha(\cos\,\theta)\right]_{\theta=\theta_2} \quad (3)$$

for the purpose of determining approximate values of ν for which the function $f_\alpha^{(\theta_1,\theta_2)}(\nu)$ vanishes (yielding a set of eigenvalues for each fixed value of α). A null searching routine (using Mathematica) then gives further precision for the zeros associated with each discrete value of degree ν. To our knowledge, analytical solutions giving values of ν that will cause (3) to vanish are not available.

In Fig. 4, we plot $f_\alpha^{(\theta_1,\theta_2)}(\nu)$ for $\alpha = 1.38037$ and note that there are zero crossings at: $\nu \cong 0.38037$, 1.43059, 7.13031, …. Plots of (3) for orders of zero and integer multiples of 1.38037 using 2, 3, 4… result in higher zero crossings than 1.43059 and have been omitted in the interest of graphical clarity. An analysis of the associated Legendre function pair (Section 5) will show why the first zero crossing must be ignored and why the selection of the associated Legendre function pair in (2) is responsible for this spurious result.

Observing (2), it is noted that both E_θ and E_ϕ require derivatives with respect to r. Additionally, E_θ and E_ϕ are both tangent to the ground plane (located at $r = a$) and at the patch (located at $r = b$). The boundary conditions that the tangent electric fields vanish on the ground plane (located at $r = a$) and the patch (located at $r = b$) are determined by zero crossings of

$$h_\nu^{(a,b)}(x) = \left[\frac{\mathrm{d}}{\mathrm{d}x}\hat{j}_\nu(x)\right]\left[\frac{\mathrm{d}}{\mathrm{d}x}\hat{y}_\nu\left(\frac{b}{a}x\right)\right] - \left[\frac{\mathrm{d}}{\mathrm{d}x}\hat{j}_\nu(x)\right]\left[\frac{\mathrm{d}}{\mathrm{d}x}\hat{y}_\nu\left(\frac{b}{a}x\right)\right] \quad (4)$$

Note we have changed the variable r to x and let $k\,a = x$ in (4), for plotting purposes.

Our analytical study will now use the 'second lowest degree' (designated $\nu_0 = 1.43059$) in Fig. 4 substituted into (4) for the purpose of determining vanishing solution (i.e. eigenvalues for x). An analysis of $h_{\nu_0}^{(a,b)}(x)$ (that is, a plot and null search for further precision) determines that the first zero crossing is at $x = 1.8604$. We indicate by X'_{α_0,ν_0}, the first zero crossing of x associated with $h_{\nu_0}^{(a,b)}(x)$ for the fixed values of α_0 and ν_0 seen in Fig. 4. The lowest resonant frequency corresponding to the first zero crossing is

$$f_{\alpha_0,\nu_0} = \frac{c}{2\pi a\sqrt{\varepsilon_\mathrm{r}}}X'_{\alpha_0,\nu_0} \quad (5)$$

where c is the speed of light in free space and ε_r is the relative dielectric constant of the material between the patch and the ground plane.

Owing to an air pocket between the PETG and the patch, this dielectric constant was volume averaged resulting in an effective value of $\varepsilon_r = 1.8$. A detailed discussion of the air gap and the volume average may be found in [12]. Accordingly, the analytically predicted resonant frequency, using (5) was found to be 432 MHz in close agreement with the measured result presented in [10–12] and shown in Fig. 3. This is the resonance along the azimuthal span of the antenna.

As a quick reality check, one can compare this resonance to the lowest resonance of a planar rectangular patch antenna [13, p. 830, (14–31)]. The longest sides of the rectangular patch antenna would be bound between the longest arc lengths of the spherical annular-sector patch approximately given by $\phi_1 a\sin\,\theta_1$ and $\phi_1 a\sin\,\theta_2$ or 20.56 and 30.43 cm, respectively. Calculation of the lowest resonant frequencies for a rectangular patch (with $\varepsilon_r = 1.8$) using these lengths predict the lowest resonant frequency in the range of 367 MHz $< f <$ 543 MHz. The measured resonance of 442 MHz for the spherical annular-sector antenna is within these bounds. With the elevation angle fixed at the centre of the patch, the arc length becomes $\phi_1 a\sin((\theta_1+\theta_2)/2)$ corresponding to an angular span of 26.10 cm. Using this angular span as the length of a rectangular patch, the calculated resonant frequency is found to be 428 MHz – reasonably close to the measured value.

We note that at resonance, the fields underneath the patch are dominated by the modal term and not by the probe location; although the probe location is important for a good impedance match [1]. Our measured resonances closely match our numerically determined resonances from our analytic procedure. We note that the analytically determined resonance associated with the lowest zero of (4), as determined using $\nu_x = 0.38037$ of Fig. 4 (i.e. 168 MHz), 'was not experimentally observed' and falls well outside the lower bound of 367 MHz using the planar patch analogy.

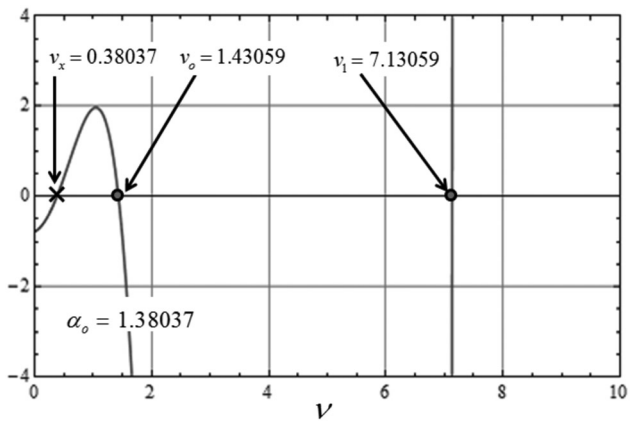

Fig. 4 *Plot of $f_\alpha^{(\theta_1,\theta_2)}(\nu)$ displays zero crossings for fixed order of $\alpha_0 = 1.38037$*

4 One source of spurious source-free resonance solutions

The failure to observe a measured resonant frequency corresponding to the degree of $\nu_x = 0.38037$ (when the order is fixed to be $\alpha_0 = 1.38037$) prompted a detailed study of the rationale for choosing the associated Legendre function pair seen in (2) [16]. For example, if the associated Legendre functions are linearly dependent, then, $P_{\nu_o}^{\alpha_o}(\cos\,\theta) = cQ_{\nu_o}^{\alpha_o}(\cos\,\theta)$ where c is a constant and (3) is trivially equal to zero. For such a case, the entire justification for the selection of the associated Legendre function pair needs re-examination and an alternate pair of associated Legendre functions would be required. This turns out to be the problem. Accordingly, we now outline a systematic procedure that may be employed once an antenna geometry is defined (e.g. a spherical cap, sector,

annulus or annular-sector); although the spherical annular-sector remains as the case study of this paper. Key to the selection procedure of the associated Legendre function pair is the analysis of linear dependency given the possible values of degree and order that unfold for the prescribed geometry of the antenna.

We now show that it was the selection of the linearly independent associated Legendre functions $P_\nu^\alpha(x)$ and $Q_\nu^\alpha(x)$ that resulted in the spurious solution indicated in Fig. 4 establishing that this solution resulted from the functions being linearly dependent. It is well known that linear dependence is indicated by a vanishing Wronskian [17]. To this end, important insight is gained by examination of the Wronskian for the associated Legendre function pair as expressed in terms of the gamma function $\Gamma(x)$. One has [15, (14.2.4)]

$$W\left(P_\nu^\alpha(x),\ Q_\nu^\alpha(x)\right) = \frac{\Gamma(\nu+\alpha+1)}{\Gamma(\nu-\alpha+1)(1-x^2)} \tag{6}$$

where $\Gamma(x) = \int_0^\infty t^{x-1}\,\mathrm{e}^{-t}\,\mathrm{d}t$ for $\mathrm{Re}(x) > 0$. When $\mathrm{Re}(x) \le 0$, $\Gamma(x)$ is defined by analytic continuation.

The Wronskian (6) will vanish if $\nu - \alpha$ equals any negative integer because the magnitude of the gamma function in the denominator will become infinite. This is exactly what occurs in the analysis of our antenna. The plot in Fig. 4 indicates a zero crossing when $\alpha = 1.38037$ (held fixed for the plot) and $\nu = 0.38037$. For these values, the magnitude in the denominator of (6) becomes infinite causing the Wronskian to vanish – indicating linear dependence. Consequently, the first zero crossing seen in Fig. 4 is not meaningful. Indeed, if ν–α equals any negative integer, linearly dependent zero crossings will occur. See Appendix 1 for further discussion of this linear dependence.

It is worth noting that when integer values of degree and order are used in (6), $\nu = n = 0,\ 1,\ 2\ldots$ and $\alpha = m = 0,\ \pm 1, \ldots, \pm n$ the associated Legendre function pair becomes $P_n^m(x)$ and $Q_n^m(x)$ and the requirement that $-n \le m \le n$ ensures a non-vanishing Wronskian with respect to the degree and order indicating the selected pair will always yield linearly independent solutions. However, for cases where non-integer degrees and orders are needed, there is no corresponding requirement that the degree ν be greater than or equal to the magnitude of the order α.

Having established that our initial choice of $P_\nu^\alpha(x)$ and $Q_\nu^\alpha(x)$ leads to a spurious solution after consideration of (6), we consider another pair. For example, an alternative associated Legendre function pair is: $P_\nu^{-\alpha}(x)$ and $Q_\nu^\alpha(x)$. This pair has the Wronskian [15, (14.2.6)]

$$W\left(P_\nu^{-\alpha}(x),\ Q_\nu^\alpha(x)\right) = \frac{\cos(\alpha\pi)}{(1-x^2)} \tag{7}$$

This Wronskian indicates the pair is useful as long as the order α is not equal to odd integer multiples of ½. Our antenna precludes these values, since $\alpha = m\pi/\phi_2 \cong 1.38037\,m$, where $m = 1,\ 2,\ \ldots$. The values of the degree cannot cause the Wronskian (7) to vanish, so this is a suitable pair for the annular-sector patch antenna under study. We now use

$$\begin{aligned} A_r = \sum_{\nu\in\nu'}\sum_{\alpha\in\alpha'} A_{\alpha\nu}&\left(C_1\cos(\alpha\phi) + C_2\sin(\alpha\phi)\right) \\ &\times\left(C_3 P_\nu^{-\alpha}\cos(\theta) + C_4 Q_\nu^\alpha\cos(\theta)\right) \\ &\times\left(C_5\hat{j}_\nu(kr) + C_6\hat{y}_\nu(kr)\right) \end{aligned} \tag{8}$$

for the analysis instead of (2). Instead of (3), we now use our alternative associated Legendre pair and plot (using Mathematica) the function

$$\begin{aligned} g_\alpha^{(\theta_1,\theta_2)}(\nu) = &\left[\frac{\mathrm{d}}{\mathrm{d}\,\theta}P_\nu^{-\alpha}(\cos\,\theta)\right]_{\theta=\theta_1}\left[\frac{\mathrm{d}}{\mathrm{d}\,\theta}Q_\nu^\alpha(\cos\,\theta)\right]_{\theta=\theta_2} \\ &-\left[\frac{\mathrm{d}}{\mathrm{d}\,\theta}Q_\nu^\alpha(\cos\,\theta)\right]_{\theta=\theta_1}\left[\frac{\mathrm{d}}{\mathrm{d}\,\theta}P_\nu^{-\alpha}(\cos\,\theta)\right]_{\theta=\theta_2} \end{aligned} \tag{9}$$

for the first four integer multiples of α with assurance that all displayed zero crossings are valid, Fig. 5. The lowest value of ν is ~1.43059 (the 'second zero' of Fig. 4, but the first zero of Fig. 5). Following the analysis of Section 4 in which we used this value for the degree, we arrive at an analytically calculated resonance in agreement with measurement. Note the absence of spurious zero crossings as compared with Fig. 4.

The solution of (4) led directly to the analytically calculated resonance that was verified by measurement for the spherical annular-sector patch antenna. An interesting parallel exists between the solution of the patch antenna resonant frequency using (4) and (5) and Schumann's solution for the resonances between the earth and the ionosphere when both the earth and ionosphere are treated as perfect conductors. Schumann found [18, p. 117, (4–201)] that the observed peaks in the frequency spectrum of noise power generated by lightning around the earth are closely estimated by

$$f_r = \frac{c}{2\pi R}\sqrt{n(n+1)}, \quad n = 1,\ 2,\ 3,\ \ldots \tag{10}$$

where R is the radius of the earth and n is the degree of associated Legendre function. Indeed, the resonance of the patch antenna is written as

$$f_{\alpha_0,\nu_0} = \frac{c}{2\pi a\sqrt{\varepsilon_r}}\sqrt{\nu_0(\nu_0+1)} \tag{11}$$

Comparing (11) with (5), it is clear that X'_{α_0,ν_0} is closely approximated by $\sqrt{\nu_0(\nu_0+1)}$. Accordingly, the calculated resonance using (11) is 433 MHz in close agreement with the 432 MHz calculation using (5). The development of (11) is presented in Appendix 2.

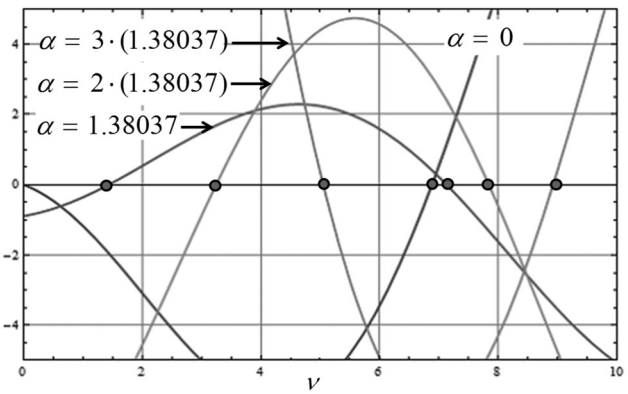

Fig. 5 *Plot of $g_\alpha^{(\theta_1,\theta_2)}(\nu)$ to determine zero crossings*

doi: 10.1049/iet-map.2014.0163

5 Conclusions

A solution for the resonant modes of a patch antenna using the cavity model on a curved (spherical) ground plane has been examined and verified by experimental measurement. An important subtlety was observed in the choice of linearly independent associated Legendre functions. Careful observation of the Wronskians and the implications for certain values of α and ν were clarified in the analytical analysis of a spherical annular-sector antenna. For such antennas, the degree and order of the associated Legendre functions often do not have integer values and plots of relevant transcendental functions may indicate spurious zero crossings that are because of the associated Legendre functions being linearly dependent. The common choice of $P_\nu^\alpha(\cos\theta)$ and $Q_\nu^\alpha(\cos\theta)$ was found to give both linearly dependent and independent solutions when trying to solve for the zero crossings of (3) for the antenna analysed in this paper. Guided by a known Wronskian, the choice of $P_\nu^{-\alpha}(\cos\theta)$ and $Q_\nu^\alpha(\cos\theta)$ was then graphed and only linearly independent zero crossings were found – leading to calculation of resonant frequencies in agreement with measurement. We view the reconciliation of the analytical frequency predictions with measured data as an important result of this paper.

Although the specific case of a spherical annular-sector patch antenna having magnetic walls about its perimeter was examined in this paper, the extension of this procedure to other canonical shapes, such as the spherical cap, spherical ring and spherical sector with various combinations of magnetic and electric walls, now poses no particular difficulty. For example, should an application require different canonical spherical shape with mixtures of boundary conditions (e.g. combinations of electric and magnetics walls), an organised analytical procedure may now be followed. Firstly, it is always possible to determine the discrete values for the order α analytically. From these set values of the order, the Wronskian for the Legendre function pair is examined to ensure that the order in (7) or combinations of the order and degree in (6) do not lead to spurious solutions. With known values of degree (determined graphically with further precision using a null searching routine), the resonant frequencies are then found using (11). Finally, we note that other associated Legendre function pairs are available, but were not discussed in this paper (e.g. $P_\nu^{-\alpha}(\cos\theta)$ and $P_\nu^{-\alpha}(\cos\theta)$) for which the associated Wronskian may be found in [15]. It is the application and mixture of boundary conditions that will lead a researcher to an optimal pair.

6 Acknowledgment

The authors would like to thank Professor Walter K. Kahn for his comments on this paper.

7 References

1 Lo, Y.T., Solomon, D., Richards, W.F.: 'An improved theory of microstrip antennas with applications', *IEEE Trans. Antennas Propag.*, 1981, **29**, (1), pp. 38–46
2 Wong, K.L.: 'Design of nonplanar microstrip antennas and transmission lines' (John Wiley & Sons, New York, 1999)
3 Tam, W.Y., Luk, K.M.: 'Resonance in spherical–circular microstrip structures', *IEEE Trans. Microw. Theory Tech.*, 1991, **39**, (4), pp. 356–357
4 Luk, K.M., Tam, W.Y.: 'Patch antennas on a spherical body', *Microw. Antennas Propag. IEE Proc. H*, 1991, **138**, (1), pp. 103–108
5 Krowne, C.M., Kuang-Yuh, W.: 'Radiation efficiency for spherical rectangular microstrip antenna'. IEEE Int. Symp. on Antennas and Propagation (IEEE AP-S), 1982, **20**
6 Kuang-Yuh, W., Kauffman, J.F.: 'Radiation pattern computations for spherical–rectangular microstrip antennas'. IEEE Int. Symp. on Antennas and Propagation (IEEE AP-S), 1983, **21**
7 Zvonimir, S., Burum, N., Bartolic, J.: 'Analysis of rectangular microstrip patch antennas on spherical surfaces', *Microw. Opt. Technol. Lett.*, 2003, **36**, (4), pp. 276–280
8 Burum, N., Zvonimir, S., Bartolic, J.: 'Mutual coupling between spherical–rectangular microstrip antennas', *Microw. Opt. Technol. Lett.*, 2004, **40**, (5), pp. 387–391
9 Weiss, S., Amang, B., Wilkins, G.M.: 'Measured, simulated, and analytical fields radiated by patch antennas conformal to spherical geometries'. IEEE Int. Symp. on Antennas and Propagation (IEEE AP-S), Spokane, July 2011
10 Boliong, A., Wilkins, G.M., Weiss, S.: 'Analytical and simulated resonances of a helmet-mounted conformal patch antenna'. IEEE Int. Symp. on Antennas and Propagation (IEEE AP-S), Chicago, July 2012
11 Boliong, A., Wilkins, G.M., Weiss, S.: 'Theoretical analysis and experimental measurements for resonant modes of patch antennas over spherical ground antenna'. 36th Ant. App. Symp. 18–20 September, Robert Allerton Park, Monticello, IL, 2012
12 Boliong, A.: 'Analytical model of a helmet-mounted conformal patch antenna for an assortment of canonical shapes'. Doctoral dissertation, Morgan State University, Baltimore, MD, 2012
13 Balanis, C.A.: 'Advanced engineering electromagnetics' (John Wiley & Sons, New York, 1989)
14 Harrington, R.F.: 'Time harmonic electromagnetic fields' (McGraw-Hill, Classic Textbook Reissue, 1987)
15 Olver, F., Lozier, D., Boisvert, R., *et al.*: 'NIST handbook of mathematical functions' (Cambridge University Press, New York, 2010)
16 Weiss, S.J.: 'Resonant patch antennas on spherical ground planes and the need for fractional order associated Legendre functions'. Radio Science Meeting (USNC-URSI NRSM), Boulder, January 2013
17 Morse, P.M., Feshbach, H.: 'Methods of theoretical physics' (McGraw-Hill, New York, 1953), pp. 524–525
18 Ishimaru, A.: 'Electromagnetic wave propagation, radiation, and scattering' (Prentice-Hall, New Jersey, 1991)
19 Arfken, G., Weber, H., Harris, F.: 'Mathematical methods for physicists' (Elsevier Academic Press, Waltham, MA, 2013, 7th edn.), p. 362
20 Lima, A., Descardeci, J., Giarola, A.: 'Microstrip antenna on a spherical surface'. IEEE Int. Symp. on Antennas and Propagation (IEEE AP-S), 1991

8 Appendix

8.1 Appendix 1

The Wronskian (6) indicates that the associated Legendre function pair $P_\nu^\alpha(x)$ and $Q_\nu^\alpha(x)$ are linearly dependent if $\nu-\alpha$ equals any negative integer. More insight as to why these particular values of degree and order lead to linear dependence from a different standpoint can be gained in considering the definitions of these functions in terms of Gauss hypergeometric functions ${}_2F_1$ as given in [15, (14.3.11)–(14.3.14)] reinforcing the need to consider alternative pairs

$$P_\nu^\alpha(x) = \cos\left(\frac{1}{2}(\nu+\alpha)\pi\right) w_1(\nu,\ \alpha,\ x) + \sin\left(\frac{1}{2}(\nu+\alpha)\pi\right) w_2(\nu,\ \alpha,\ x) \tag{12}$$

$$Q_\nu^\alpha(x) = -\frac{1}{2}\pi\sin\left(\frac{1}{2}(\nu+\alpha)\pi\right) w_1(\nu,\ \alpha,\ x) + \frac{1}{2}\pi\cos\left(\frac{1}{2}(\nu+\alpha)\pi\right) w_2(\nu,\ \alpha,\ x) \tag{13}$$

where (see (14) and (15))

Note that

$$\left|1/\Gamma\left(\frac{1}{2}v-\frac{1}{2}\alpha+1\right)\right|_{v-\alpha\to-2,-4,-6,\ldots}\to 0 \quad (16)$$

$$\left|1/\Gamma\left(\frac{1}{2}v-\frac{1}{2}\alpha+1\right)\right|_{v-\alpha\to-1,-3,-5,\ldots}\to 0 \quad (17)$$

Substituting (16) into (14) and (17) into (15), we arrive at

$$P_v^{\alpha}(x)\big|_{v-\alpha=-2,-4,-6,\ldots}=\sin\left(\frac{1}{2}(v+\alpha)\pi\right)w_2(v,\ \alpha,\ x) \quad (18)$$

$$Q_v^{\alpha}(x)\big|_{v-\alpha=-2,-4,-6,\ldots}=\frac{1}{2}\pi\cos\left(\frac{1}{2}(v+\alpha)\pi\right)w_2(v,\ \alpha,\ x) \quad (19)$$

and

$$P_v^{\alpha}(x)\big|_{v-\alpha=-1,-3,-5,\ldots}=\cos\left(\frac{1}{2}(v+\alpha)\pi\right)w_1(v,\ \alpha,\ x) \quad (20)$$

$$Q_v^{\alpha}(x)\big|_{v-\alpha=-1,-3,-5,\ldots}=\frac{1}{2}\pi\cos\left(\frac{1}{2}(v+\alpha)\pi\right)w_1(v,\ \alpha,\ x) \quad (21)$$

For fixed order and degree with the constraint of (16), the associated Legendre function pair in (12) and (13) become (18) and (19), respectively, where both are dependent on $w_2(v,\ \alpha,\ x)$. The constraint of (17) causes (12) and (13) to become the pair of (20) and (21), respectively, where both are dependent on $w_1(v,\ \alpha,\ x)$. Accordingly, the pair must be linearly dependent functions of x when the difference between the degree and order form a negative integer.

8.2 Appendix 2

Under the condition that $k(b-a)\ll 1$, a careful analysis of the vanishing of (4) leads directly to (11). The analytical details are presented in this Appendix. As a preliminarily comment, we note the Schelkunoff's spherical Bessel functions solve the differential equation [13, p. 551, (10–32)]

$$\left[\frac{\mathrm{d}^2}{\mathrm{d}\,r^2}+k^2-\frac{v(v+1)}{r^2}\right]\hat{b}_v(kr)=0 \quad (22)$$

where $\hat{b}_v(kr)$ represents either $\hat{j}_v(kr)$ or $\hat{y}_v(kr)$. The absence of a first-order derivative in (22) indicates that the Wronskian of $\hat{j}_v(kr)$ and $\hat{y}_v(kr)$ is equal to a non-zero constant [19, p. 362, (7.62)], namely

$$W(\hat{j}_v(kr),\ \hat{y}_v(kr))=\text{const} \quad (23)$$

Having made this preliminary comment, we now turn our attention to an approximate solution for which (4) vanishes. To this end, we rewrite (4) as

$$\hat{j}_v'(ka)\hat{y}_v(kb)-\hat{j}_v'(kb)\hat{y}_v(ka)=0 \quad (24)$$

In (24), the prime notation indicates a derivative with respect to the argument of the function. The derivatives of the Schelkunoff functions may now be expanded into a power series about a

$$\hat{j}_v'(kr)=\hat{j}_v'(ka)+\hat{j}_v''(ka)(k(r-a))^1+\frac{1}{2!}\hat{j}_v'''(ka)(k(r-a))^2+\ldots \quad (25)$$

$$\hat{y}_v'(kr)=\hat{y}_v'(ka)+\hat{y}_v''(ka)(k(r-a))^1+\frac{1}{2!}\hat{y}_v'''(ka)(k(r-a))^2+\ldots \quad (26)$$

Evaluating (25) and (26) at $r=b$, we obtain the following approximations, under the condition that $k(b-a)\ll 1$

$$\hat{j}_v'(kb)\cong\hat{j}_v'(ka)+\hat{j}_v''(ka)(k(b-a))^1 \quad (27)$$

$$\hat{y}_v'(kb)\cong\hat{y}_v'(ka)+\hat{y}_v''(ka)(k(b-a))^1 \quad (28)$$

Substituting (27) and (28) into (24) and simplifying, we obtain

$$\hat{j}_v'(ka)\hat{y}_v''(ka)-\hat{j}_v''(ka)\hat{y}_v'(ka)=0 \quad (29)$$

Here it is recognised, from (22), that

$$\hat{j}_v''(ka)=-\left(k^2-\frac{v(v+1)}{a^2}\right)\hat{j}_v(ka) \quad (30)$$

$$\hat{y}_v''(ka)=-\left(k^2-\frac{v(v+1)}{a^2}\right)\hat{y}_v(ka) \quad (31)$$

Substituting (30) and (31) into (29) and simplifying, we arrive at

$$\left[\hat{j}_v'(ka)\hat{y}_v(ka)-\hat{j}_v(ka)\hat{y}_v'(ka)\right]\times\left(k^2-\frac{v(v+1)}{a^2}\right)=0 \quad (32)$$

The term in the square brackets of (32) is recognised as the Wronskian which we know from (23) is a non-zero constant. Accordingly, (32) may be solved for k

$$k=\frac{1}{a}\sqrt{v(v+1)} \quad (33)$$

Since $k=(2\pi f/c)\sqrt{\varepsilon_r}$, we obtain

$$f=\frac{c}{2\pi a\sqrt{\varepsilon_r}}\sqrt{v(v+1)} \quad (34)$$

We note a similar result was given in [6] when a proper normalisation constant for a probe-fed annular-sector antenna implied (34). However, (34) is developed independently of the excitation mechanism of the patch. Similar results have been reported for spherical patch antennas [20, p. 821 (3)].

$$w_1(v,\ \alpha,\ x)=\frac{2^{\alpha}\Gamma((v+\alpha+1)/2)}{\sqrt{\pi}\Gamma((v-\alpha+2)/2)}\ (1-x^2)^{-\alpha/2}{}_2F_1\left(-\frac{1}{2}v-\frac{1}{2}\alpha,\ +\frac{1}{2}v-\frac{1}{2}\alpha+\frac{1}{2};\ \frac{1}{2};\ x^2\right) \quad (14)$$

$$w_2(v,\ \alpha,\ x)=\frac{2^{\alpha+1}\Gamma((v+\alpha+2)/2)}{\sqrt{\pi}\Gamma((v-\alpha+1)/2)}\ x(1-x^2)^{-\alpha/2}{}_2F_1\left(+\frac{1}{2}-\frac{1}{2}v-\frac{1}{2}\alpha,\ +\frac{1}{2}v-\frac{1}{2}\alpha+1;\ \frac{3}{2};\ x^2\right) \quad (15)$$

doi: 10.1049/iet-map.2014.0163